Many-body electronic structures at transition-metal surfaces: Ni(001)

1992 J. Phys.: Condens. Matter 4 9855

(http://iopscience.iop.org/0953-8984/4/49/013)

J. Phys.: Condens. Matter 4 (1992) 9855–9868. Printed in the UK

Many-body electronic structures at transition-metal surfaces: Ni(001)

Changfeng Chen
Department of Physics, University of Nevada, Las Vegas, NV 89154, USA

Received 9 April 1992, in final form 22 September 1992

Abstract. Exact-diagonalization calculations have been performed to study the electronic structure of d band metal surfaces, with specific applications to a Ni(001) surface. Results of local-density-approximation band-structure calculations are taken as the starting point. A realistic surface model of d electrons has been constructed in a tight-binding scheme, with the strong short-range d–d correlation fully taken into account in a periodic small-cluster approach. Calculated results show some interesting features induced by many-body effects. The implications and consequences of the results are discussed.

1. Introduction

The electronic and magnetic properties of transition-metal surfaces are of interest for the understanding of a wide variety of surface phenomena: magnetization enhancement at surfaces, changes of surface properties with adsorption, as well as the properties of metal–metal and metal–semiconductor interfaces. There is a large body of literature, both experimental and theoretical, on this subject. From the theoretical point of view, the major challenge is how to treat the strongly correlated itinerant d electrons in these materials. The local-spin density functional (LSDF) method provides us with a good description for the ground-state properties of bulk as well as surfaces, interfaces and superlattices of transition metals [1]. However, despite its success, the LSDF method has some intrinsic problems in dealing with strongly correlated electron systems, such as transition metals [2–4]. There have been some attempts [5] to make improvements within the general framework of LSDF. Recently we have proposed [6, 7] to use a different approach to examine the d electron problem, in particular at reduced dimensionality where correlation effects are expected to be stronger. We take the results of band calculations as the starting point and include the many-body effect in a periodic small-cluster approach (PSCA). In PSCA the single-particle and many-body effects are treated on an equal footing. The problem is made tractable by sampling only a few high-symmetry points in the Brillouin zone. This is equivalent to selecting a finite-size crystal in real space with periodic boundary conditions; thus the name PSCA. This approach has been successfully applied to study many-body problems in various systems [6–8], where local strong interactions are important.

In the previous study [6, 7], we focused primarily on the thin-film structures of transition metals. Some conclusions on the surface properties were drawn from the calculations using free-standing thin slabs. While most of the qualitative conclusions on features induced by many-body effects at transition-metal surfaces are expected to

0953-8984/92/499855+14$07.50

remain valid, we believe that a more realistic surface model is necessary to provide a quantitatively better description and make it more sensible to compare the calculated results with experiments. It is also important to construct a realistic surface model in order to attack problems like surface adsorption, overlayer and interface properties. It is the purpose of this paper to present a surface model for transition metals, with specific applications to a Ni(001) surface, thus to extend our previous work on Ni thin films [6]. We calculate photoemission spectra of Ni(001) and study effects of the hole–hole interaction in the system. This problem in bulk Ni has been studied previously by several authors using various schemes of perturbation theory [9] and later using the exact-diagonalization method [10]. Comparison between different theories has been given in [10]. Because the d–d correlation effect in the photoemission process in 3d transition metals is intrinsically short ranged, application of the exact-diagonalization method has been quite successful.

The rest of this paper is organized as follows. In section 2, the model Hamiltonian is introduced. In section 3, the method of calculation is described. Section 4 is a discussion on the single-particle electronic structure. Section 5 presents the results of the calculated photoemission spectrum and the discussion on the many-body electronic structure. The conclusion is summarized in section 6.

2. The model Hamiltonian

In the previous study [6] of the thin-film photoemission spectrum of nickel metal, a {001} two-layer slab model was used. Here the same sampling of the surface Brillouin zone is chosen, but the slab is now connected to the bulk on one side in a tight-binding scheme, thus representing a realistic {001} surface structure at the single-particle level. The periodic boundary condition is only applied parallel to the surface. The many-body calculation is still restricted to the same four-atom tetrahedral cluster. However, the single-particle electronic structure is modified from the thin-film results by allowing the hopping of the particles between the top two layers and the bulk. This one-electron calculation provides a better starting point for the many-body cluster calculation of the surface structure. The following changes are introduced as a result of the presence of the surface. First, the symmetry at the surface is reduced from that of the bulk and free-standing slab. Therefore, the final Hamiltonian matrices to be diagonalized will be of higher dimensions. Second, the crystal-field effects are different because electrons near the surface experience a different local atomic environment. The change in kinetic-energy effects at the surface further modifies the single-particle band structure.

The model Hamiltonian contains both single-particle and two-particle terms:

$$H = \sum_{\substack{i,j;\mu,\nu;\sigma \\ i\neq j}} t_{i\mu,j\nu} c^{+}_{i\mu\sigma} c_{j\nu\sigma} + \sum_{i;\mu;\sigma} E_{\mu} c^{+}_{i\mu\sigma} c_{i\mu\sigma} + \sum_{i;\mu,\nu,\lambda,\phi;\sigma,\sigma'} V_{\mu\nu\lambda\phi} c^{+}_{i\mu\sigma} c^{+}_{i\nu\sigma'} c_{i\lambda\sigma'} c_{i\phi\sigma} \tag{2.1}$$

where ij label atoms in the cluster; μ, ν, λ, ϕ label the five d orbitals; σ, σ' are spin labels.

The single-particle hopping terms $t_{i\mu j\nu}$ are parametrized according to the Slater–Koster scheme [11]. The tetrahedral cluster chosen here allows only nearest-neighbour hopping; in the restricted crystal the second-nearest neighbour of an atom is identical to itself. Only d electrons are *explicitly* included in the calculation. The s-like conduction band of nickel metal is treated as an electron reservoir which has 'absorbed' two electrons per cluster, leaving two d holes in the four-atom cluster, i.e. 0.5d hole per atom. This is the closest possible value to the theoretical [12] and experimental [13] estimates of 0.56 hole per atom, since the method used here allows only an integral number of particles in the cluster. The s–d hybridization and the d–d interaction beyond the nearest neighbours are taken into account by adjusting the d orbital energies to fit the results of all-electron band-structure calculations. The single-particle parameters are further adjusted to account for the modifications at the surface as discussed above. The d orbitals characterized by these parameters are then used in the many-body cluster calculation.

The intra-atomic Coulomb interactions $V_{\mu\nu\lambda\phi}$ most generally allowed by atomic symmetry [14] are used. They include a direct Coulomb integral U, an average exchange integral J and an exchange anisotropy ΔJ. The value is chosen to be 4.3 eV following the bulk calculation [10] and the other parameters are set in the ratios $U:J:\Delta J = 56:8:1$ based on the consideration of constraints imposed by atomic data and the screening effects in metals. It is expected that the value of U may increase at surfaces due to the more localized character of d electrons at reduced dimensionality. However, it has been found that a variation in U in the range of a few eV does not cause any substantial change in the calculated results. Due to this insensitivity of the calculated results to the value of U, there is no need here to actually adjust the bulk U to a more realistic surface U [15].

In the thin-film work [6] we have performed a crystal-field analysis. In the present surface structure, the energy shift of the five d orbitals are modified due to the change of local atomic environment. For atoms in the top (surface) layer, one has

$$\Delta E_{\alpha 1} = -(\tfrac{7}{15})d_{1n} + (\tfrac{4}{3})d_{2n} \tag{2.2}$$

$$\Delta E_{\beta 1} = -(\tfrac{17}{15})d_{1n} + (\tfrac{8}{3})d_{2n} \tag{2.3}$$

$$\Delta E_{\gamma 1} = (\tfrac{28}{15})d_{1n} - (\tfrac{4}{3})d_{2n} \tag{2.4}$$

$$\Delta E_{\delta 1} = \Delta E_{\epsilon 1} = -(\tfrac{2}{15})d_{1n} - (\tfrac{4}{3})d_{2n} \tag{2.5}$$

and for the second layer (the 'bulk-like' one, except that each atom has only five second neighbours instead of six in the true bulk environment [16])

$$\Delta E_{\alpha 2} = -(\tfrac{6}{5})d_{1n} + (\tfrac{4}{3})d_{2n} \tag{2.6}$$

$$\Delta E_{\beta 2} = -(\tfrac{6}{5})d_{1n} + (\tfrac{8}{3})d_{2n} \tag{2.7}$$

$$\Delta E_{\gamma 2} = \Delta E_{\delta 2} = \Delta E_{\epsilon 2} = (\tfrac{4}{5})d_{1n} - (\tfrac{4}{3})d_{2n} \tag{2.8}$$

where the subscripts $\alpha 1$, $\beta 1$, $\gamma 1$, $\delta 1$, $\epsilon 1$ refer to the five d orbitals of symmetries $(r^2 - 3z^2)$, $(x^2 - y^2)$, xy, yz, zx in the top layer and $\alpha 2$, $\beta 2$, $\gamma 2$, $\delta 2$, $\epsilon 2$ refer to the five d orbitals in the second ('bulk-like') layer. The contribution to the energy

Table 1. Hamiltonian parameters (energies are in eV *below* the Fermi level of bulk Ni metal). The subscripts $\alpha 1$, $\beta 1$, $\gamma 1$, $\delta 1$, and $\epsilon 1$ refer to the five d orbitals of symmetries $(r^2 - 3z^2)$, $(x^2 - y^2)$, xy, yz and zx in the top layer of the surface structure, and $\alpha 2$, $\beta 2$, $\gamma 2$, $\delta 2$, and $\epsilon 2$ refer to the same d orbitals in the second layer.

$(dd\sigma)$	0.446
$(dd\pi)$	−0.335
$(dd\delta)$	0.098
$E_{\alpha 1}$	2.234
$E_{\beta 1}$	2.680
$E_{\gamma 1}$	0.267
$E_{\delta 1}$	2.417
$E_{\epsilon 1}$	2.417
$E_{\alpha 2}$	3.022
$E_{\beta 2}$	2.752
$E_{\gamma 2}$	1.414
$E_{\delta 2}$	1.414
$E_{\epsilon 2}$	1.414
U	4.30
J	0.614
ΔJ	0.077

shift from each of the first and second neighbours d_{1n} and d_{2n} have already been determined in the bulk crystal-field analysis [6].

All the Hamiltonian parameters for the surface structure are summarized in table 1. Energies are measured below the Fermi level of bulk nickel metal. The crystal-field induced d-orbital energy shifts are calculated such that the centre of gravity of the d manifold is kept unchanged.

3. Method of calculation

With five d orbitals per atom per spin, there are 40 orbitals in the four-atom cluster. Simple combinatorial arguments yield 780 states for two holes in the neutral state of the cluster. The photoemission process adds a third hole to the cluster, yielding 9880 final states. Clearly, symmetries inherent in the Hamiltonian (2.1) must be exploited in order to diagonalize the Hamiltonian matrix. First, total spin in the cluster is a good quantum number. For the case of two holes in the cluster, there are 190 triplets and 210 singlets. For the case of three holes in the cluster, there are 1140 quartets and 2260 doublets. These spin states, with the exception of the singlets, can be divided into states with different total z-component S_z, which is also a good quantum number. Here this symmetry simply causes the degeneracy for the states of the same S but different S_z. Therefore, in the calculations it is enough to include explicitly only those states with the highest S_z. Furthermore, there is a space-group decomposition which is very efficient in reducing the matrix size.

The space group of the surface structure discussed above is symmorphic of order 8, a reduction by a factor of 2 from that of the thin-film structure [6]. It is the direct product of the point group C_4 and the finite translational group $T = \{0, \tau\}$, where τ is the vector connecting the two sites in the surface layer in the cluster. This symmorphic space group possesses eight irreducible representations; all of them

are one-dimensional, four at $\bar{\Gamma}$ and four at $\bar{X}$. These $\bar{\Gamma}$ and $\bar{X}$ representations, labelled by the translational group k vectors, correspond to the following points of the two-dimensional square-surface Brillouin zone (which extends over the region $-2\pi/a < \pm k_x \pm k_y < 2\pi/a$):

$$(0,\ 0) \text{ for } \bar{\Gamma} \tag{3.1}$$

$$(2\pi/a,\ 0) \text{ for } \bar{X} \tag{3.2}$$

where a is the cubic lattice constant of the FCC structure. These two points constitute the finite sampling of the reciprocal space inherent in the PSCA. The character table of the group [17] is given in table 2. The irreducible representations listed above can be connected to those of the thin-film structure and bulk FCC structures via compatibility relations. These relations are given in table 3; they govern the manner of splitting or combination of these states when symmetry reduction or increment occurs.

Table 2. The character table of the four-atom-cluster symmorphic space group for the {001} FCC surface structure. Representations with braces are degenerate because of time-reversal symmetry. The vector τ is the translation connecting the two sites in the same layer in the cluster.

	E	C_4	C_2	C_4^{-1}	$\{E\|\tau\}$	$\{C_4\|\tau\}$	$\{C_2\|\tau\}$	$\{C_4^{-1}\|\tau\}$
$\bar{\Gamma}_1$	1	1	1	1	1	1	1	1
$\bar{\Gamma}_2$	1	−1	1	−1	1	−1	1	−1
$\bar{\Gamma}_3$	1	i	−1	−i	1	i	−1	−i
$\bar{\Gamma}_4$	1	−i	−1	i	1	−i	−1	i
$\bar{X}_1$	1	1	1	1	−1	−1	−1	−1
$\bar{X}_2$	1	−1	1	−1	−1	1	−1	1
$\bar{X}_3$	1	i	−1	−i	−1	−i	1	i
$\bar{X}_4$	1	−i	−1	i	−1	i	1	−i

With a complete set of matrices that transform according to these irreducible representations, it is possible to project out sets of symmetrized basis states. The grand orthogonal theorem and the matrix-element theorem guarantee that the Hamiltonian matrix will be in block diagonal form (with no mixing between states of different spin or spatial symmetry), when it is expanded in a symmetrized basis that has definite spin and transforms like the (1,1) elements of an irreducible representation of the symmetry group [18]. In the case of representations that have complex-valued (1,1) elements the projection is onto the subspace spanned by the complex representation and its conjugate so that all matrix elements are real. The price for having all-real matrix elements is that the size of the block corresponding to that particular representation is doubled. One might have to avoid this scheme and introduce a complex-valued version of the projection procedure as the calculations really approach the limit of the computational power available. This is not the case in the present work.

A symmetry-adapted computer (integer) algorithm was used to construct the projection operators from the matrix elements of the irreducible representations and operate on states with maximum total z-component of spin to generate symmetrized

Table 3. Compatibility relations between the representations of the space groups for the bulk, thin-film and surface structures. The bulk and thin-film representations are given in [22] and [6] respectively. The representations in parentheses indicate the thin-film-to-surface splitting pattern (only the non-obvious ones are explicitly indicated).

Representations of the bulk structure	Representations of the thin-film structure	Representations of the surface structure
Γ_1	γ_1	$\bar{\Gamma}_1$
Γ_2	γ_3	$\bar{\Gamma}_2$
Γ_{12}	$\gamma_1 + \gamma_3$	$\bar{\Gamma}_1 + \bar{\Gamma}_2$
Γ'_{15}	$(\gamma_2) + \gamma_5$	$(\bar{\Gamma}_1) + \bar{\Gamma}_3 + \bar{\Gamma}_4$
Γ'_{25}	$(\gamma_4) + \gamma_5$	$(\bar{\Gamma}_2) + \bar{\Gamma}_3 + \bar{\Gamma}_4$
X_1	$\gamma_2 + x_5$	$\bar{\Gamma}_1 + \bar{X}_1 + \bar{X}_2$
X_2	$\gamma_4 + x_5$	$\bar{\Gamma}_2 + \bar{X}_1 + \bar{X}_2$
X_3	$\gamma_3 + (x_1) + x_2$	$\bar{\Gamma}_2 + (\bar{X}_3) + \bar{X}_4$
X_4	$\gamma_1 + x_1 + x_2$	$\bar{\Gamma}_1 + \bar{X}_3 + \bar{X}_4$
X_5	$\gamma_5 + (x_3) + x_4 + x_5$	$\bar{\Gamma}_3 + \bar{\Gamma}_4 + \bar{X}_1 + \bar{X}_2 + \bar{X}_3 + (\bar{X}_4)$

Table 4. Sizes of blocks of the various irreducible representations for the surface-structure space group. Due to the all-real-value projection procedure used in the calculations (see the text for details), the block sizes of the representations $\bar{\Gamma}_3(\bar{\Gamma}_4)$ and $\bar{X}_3(\bar{X}_4)$ are doubled; the actually calculated largest block is of order 660.

		$\bar{\Gamma}_1$	$\bar{\Gamma}_2$	$\bar{\Gamma}_3$	$\bar{\Gamma}_4$	$\bar{X}_1$	$\bar{X}_2$	$\bar{X}_3$	$\bar{X}_4$
$N = 2$	$S = 1$	21	21	24	24	26	26	24	24
	$S = 0$	33	29	24	24	26	26	24	24
$N = 3$	$S = \frac{3}{2}$	140	138	146	146	139	139	146	146
	$S = \frac{1}{2}$	334	336	330	330	335	335	330	330

basis functions of definite spin and spatial symmetry. The Hamiltonian matrix blocks are determined *exactly* in this symmetrized basis and diagonalized to obtain all of the eigenvalues and eigenstates. Table 4 summarizes the reduced block sizes of various irreducible representations.

4. Single-particle electronic structures

In the thin-film case [6], we have seen that it is very important to have a thorough analysis of the single-particle electronic structure in order to interpret correctly the calculated photoemission spectrum and thus make sensible comparison with experimental results and draw correct conclusions about the many-body states in the system. The calculated single-particle energy levels of the surface structure at special symmetry points are summarized in table 5, together with the thin-film and bulk results for comparison. There are some common features in the thin-film and surface-energy spectra. They both have an energy-level split off the main body of the spectrum, which is caused by the anisotropic change of the local atomic environment experienced by the particles in various d orbitals [19] in the presence of surfaces; this split-off leads to a wider spread of the d band than in the bulk case. However, most of the d bands in the surface and thin-film case are narrower than the bulk

ones due to the more localized character of particles at reduced dimensionality. A more detailed analysis reveals that there are also some important differences between the thin-film and surface results. Due to the symmetry reduction at the surface the split-off thin-film level of X_5 symmetry now further splits into two levels of $\overline{X}_2$ and $\overline{X}_1$ symmetry, separated by 1.15 eV. These two levels are nondegenerate (except spin) and can each accommodate only one electron (or hole) of each spin.

Table 5. One-particle energy levels (energies are in eV *below* the Fermi level of bulk Ni metal) of the {001} FCC surface structure, together with the bulk and thin-film results. The numbers in parentheses are degeneracies per spin.

Surface		Thin film[a]		Bulk[b]	
Energy	Symmetry	Energy	Symmetry	Energy	Symmetry
−1.169	$\overline{X}_2(1)$	−1.223	$x_5(2)$	−0.01	$X_5(6)$
−0.022	$\overline{X}_1(1)$	1.065	$\gamma_4(1)$	0.18	$X_2(3)$
0.596	$\overline{\Gamma}_3$, $\overline{\Gamma}_4(2)$	1.173	$\gamma_4(1)$	0.92	$\Gamma_{12}(2)$
0.950	$\overline{X}_3$, $\overline{X}_4(2)$	1.396	$x_5(2)$	2.04	$\Gamma'_{25}(3)$
0.975	$\overline{X}_1(1)$	1.407	$\gamma_5(2)$	3.81	$X_3(3)$
1.063	$\overline{\Gamma}_2(1)$	1.505	$\gamma_3(1)$	4.31	$X_1(3)$
1.393	$\overline{\Gamma}_2(1)$	1.883	x_3, $x_4(2)$		
1.610	$\overline{X}_2(1)$	2.125	$\gamma_3(1)$		
1.689	$\overline{\Gamma}_2(1)$	2.367	$\gamma_5(2)$		
2.143	$\overline{\Gamma}_1(1)$	2.371	$\gamma_1(1)$		
2.284	$\overline{\Gamma}_3$, $\overline{\Gamma}_4(2)$	3.795	x_1, $x_2(2)$		
3.162	$\overline{\Gamma}_2(1)$	4.011	$\gamma_2(1)$		
3.834	$\overline{X}_3$, $\overline{X}_4(2)$	4.280	$x_5(2)$		
4.593	$\overline{\Gamma}_1(1)$				
4.612	$\overline{X}_1(1)$				
4.692	$\overline{X}_2(1)$				

[a] [6].
[b] [13].

To understand and correctly interpret the results obtained in a finite-basis calculation, a more realistic band picture is sometimes helpful and important. Similarly to the thin-film results, in the present restricted finite-basis surface case the two holes in the four-atom cluster sit on the highest *electronic* levels of $\overline{X}_2$ and $\overline{X}_1$ symmetry with the same spin orientation, i.e. in the minority-spin state, following Hund's rule. The Fermi level is thus at the $\overline{X}_2$ majority-spin level. This is actually an atomic point of view, i.e. a discrete-level picture. In fact, in a true crystalline solid, energy levels form energy bands; the top band in the surface case can accommodate four electrons (or holes) of each spin. In this case the two holes in the cluster will be in the minority-spin band, which is now half-filled. The majority-spin band is fully occupied by electrons and *below* the Fermi level. The Fermi level, on the other hand, will intersect the half-filled minority-spin band. Therefore electrons *at the Fermi level* will be only of *minority* spin, opposite to what was found in the discrete-level picture. This means that in a spin-resolved but *angle-integrated* photoemission experiment the emitted electrons with the highest kinetic energy will be of minority spin. On the other hand, the minority-spin band is only half-filled. Since the $\overline{X}$ level is at the top of the band, it is not occupied by minority-spin electrons. Thus the emitted electrons with the highest kinetic energy in an *angle-resolved* photoemission experiment with

the angle corresponding to the $\overline{X}$ point in the surface Brillouin zone should be of majority spin, as predicted in the discrete-level picture.

A general remark is now in order: while the finite-basis calculations can provide some accurate information on uniform and short-range properties, which can be referred to as 'angle-resolved' (corresponding to high-symmetry points in the reciprocal space) properties, some caution must be taken in making conclusions on angle-integrated, or long-range, properties. The band picture may help to interpret some angle-integrated properties calculated in a restricted finite basis. However, intrinsically long-range properties, such as phase transitions, are still out of reach of this type of finite-basis calculation.

5. Many-body electronic structure and photoemission spectrum

Many-body correlations modify the single-particle electronic structure and create new features uniquely related to many-body effects. Photoemission measurements provide a very useful probe of the electronic states. In its idealized realization, a single-particle picture photoemission spectrum is a direct measure of the electronic density of states. When many-body interactions are turned on, the picture becomes quite complex, because the interactions mix all one-particle levels and may cause redistribution of the spectral weights. The theoretical description and correct understanding of experimental observations require accurate many-body calculations, insightful interpretation of data and sophisticated matching of theory and experiment. The physical process involved in photoemission is intrinsically short-ranged. Therefore it should be well described in the PSCA.

For two holes in the tetrahedral cluster the Hamiltonian (2.1) yields accidentally degenerate many-body states of symmetries ${}^3\overline{\Gamma}_2$ and ${}^1\overline{\Gamma}_2$. When the nearest-neighbour exchange is considered, ${}^3\overline{\Gamma}_2$ has lower energy and is henceforth considered to be the ground state. It is found to contain only holes from the $\overline{X}_1$ and $\overline{X}_2$ one-particle levels and has zero probability of having two holes in the same site. As a consequence, there is no contribution from the on-site interactions to the ground-state energy.

The density of many-body states (MBDOS) is the best way to show the spectrum of energy eigenvalues of the Hamiltonian. At each eigenvalue [2$\bar{0}$], a peak of weight equal to the degeneracy at that energy is plotted. Figure 1 shows the MBDOS of the Ni(001) surface structure.

The photoemission process adds a third hole to the system. The one-electron density of (emitted) states is calculated by adding a hole to the two-hole ground state and projecting the result onto the eigenstates of the cluster with three holes. When a hole of particular spin and spatial symmetry is added, one obtains a spin- and angle-resolved density of states, i.e. the photoemission spectrum (PES). The results may be added to obtain the total d band PES.

The photoemission spectrum is defined as

$$F_{\mathrm{PE}}(\epsilon, \mu\sigma) = \sum_k |\langle \nu^{(k)}|c_{\mu\sigma}|\psi_0\rangle|^2 \delta(\epsilon - \epsilon^{(k)} + \epsilon_0) \tag{5.1}$$

where $|\nu^{(k)}\rangle$ is the kth eigenstate in the three-hole final-state manifold of the cluster, $|\psi_0\rangle$ is the two-hole ground state, and $\epsilon^{(k)}$ and ϵ_0 are the corresponding eigenvalues. The operator $c_{\mu\sigma}$ destroys an electron or, equivalently, creates a hole on the orbital

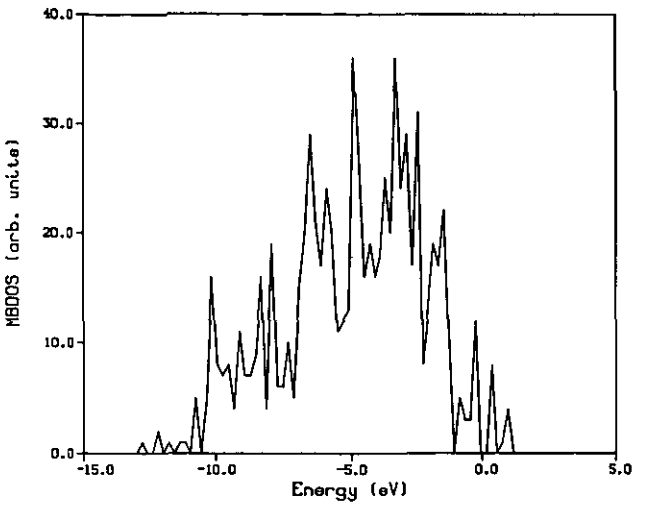

Figure 1. The eigenvalue spectrum, i.e. density of many-body states (MBDOS), of the Ni(001) surface structure.

μ (μ runs over the 20 d orbitals in the cluster) with spin σ in the ground state. From equation (5.1) one can obtain spin-, angle-, and energy-resolved as well as integrated PES results. It should be pointed out that equation (5.1) does not include the photoemitted electron state and photoexcitation factor $\boldsymbol{p} \cdot \boldsymbol{A}$. As a result, the peak profile of angle-resolved photoemission will be modified. However, the peak position of the spectrum is not affected. Furthermore, even peak intensity can be calculated reasonably well in this approach, as demonstrated in the bulk case [10] where calculated results are compared with angle-resolved (corresponding to the X point) experimental results. Nevertheless, quantitative deviation caused by this approximation does exist. In the present work, the emphasis is on the effects resulting from strong short-range electron–electron interactions, which is best handled by the approach used here.

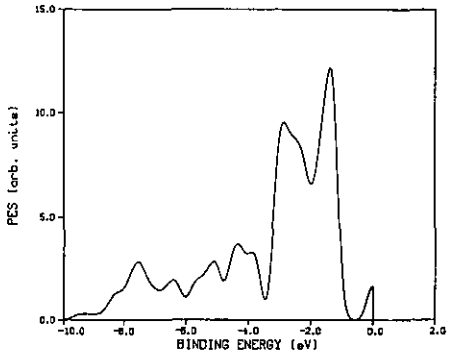

Figure 2. The total calculated photoemission spectrum (PES). The Fermi level (E_F = 0.0 eV) is determined by the surface electronic structure and raised by 1.169 eV relative to the bulk value. The location of the lowest single-electron state at $\overline{X}$ in the d band according to the single-particle calculation (see table 5) is denoted by E_b.

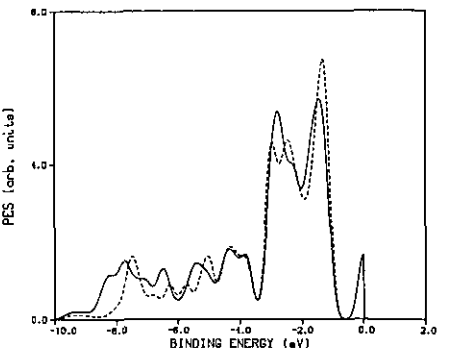

Figure 3. The total spin-resolved PES. Solid lines correspond to the majority-spin states and dashed lines the minority-spin states.

Figure 2 shows the total spin- and angle-integrated PES. Figure 3 is the total angle-integrated but spin-resolved PES. In all figures, the sharp lines characteristic of a finite system have been artificially broadened with Gaussian peaks of 0.3 eV half-width. It is obvious that the surface PES results are quite different from either the bulk or the thin-film ones. The most distinctive difference from the bulk result is the split-off peak of majority-spin character at the Fermi level. The spread of the spectrum is broader than in the bulk case; this is caused mainly by the change of the single-particle electronic structure at the surface. Another noticeable change is that the main peak in the 'main line' part (i.e. the part with energy $E > E_b$, where $E_b = -5.9$ eV is the bottom of the spectrum predicted by single-particle calculations) is much broader and has a well-resolved double-peak structure. Comparing with the thin-film results, the surface PES is somewhat bulk-like except that there is a split-off peak at the Fermi level and the main body of the spectrum shifts toward higher binding energy. Both the split-off peak at the Fermi level and satellite part of the spectrum (i.e. $E < E_b$) have lower relative intensity; the former is the result of the different split-off pattern in the single-particle electronic structure and the latter an indication of correlation effects weaker at surfaces than in the thin film where particle motions are essentially confined in the two-dimensional slab. It can be seen in the spin-resolved PES that the spin polarization of the whole spectrum is weak, with the exception of the split-off peak at the Fermi level which is fully polarized in majority-spin orientation and the high-binding-energy side of the satellite peak. These differences in gross features in the surface PES from the bulk and thin-film results suggest that a detailed investigation of the surface PES be necessary in order to understand the many-body electronic structure at transition-metal surfaces probed by the photoemission technique. Furthermore, any study of many-body effects in more complex systems involving transition-metal surfaces, e.g. adsorption and interface systems, will require a clear understanding of the properties at the clean surfaces. It is the purpose of this work to provide the insight into the problems of the many-body effects in the PES and a starting point for further studies.

A thorough analysis of the calculated results reveals some more detailed features in the PES of the Ni(001) surface. In the following we shall focus on the angle-resolved PES results.

We first present in figure 4 the total spin-resolved PES corresponding to the $\bar{\Gamma}$ point, which should be compared with normal-emission surface-sensitive photoemission experiments. There is a well-resolved double-peak structure in the spectrum; the one at lower binding energy has higher spin polarization and larger exchange splitting and the one at higher binding energy has higher intensity but little spin polarization and exchange splitting. There is no spectral weight observed with binding energy less than about 0.76 eV. There is a satellite peak at about 6.4 eV below the Fermi level with a long tail into higher binding-energy part. This peak has quite strong spin polarization in majority-spin orientation and large exchange splitting, the result of the strong correlation between the majority- and minority-spin electrons (holes).

Shown in figure 5 is the total spin-resolved PES corresponding to the $\bar{X}$ point. There are more structures in this spectrum than in the case of the $\bar{\Gamma}$ point. The most noticeable feature is the surface-induced peak at the Fermi level. It is fully polarized in majority-spin orientation. A detailed analysis of the data shows that this peak comes completely from the contribution of states of $\bar{X}_1$ symmetry. There are two broad peaks with some fine structures centred around -1.9 eV and -4.5 eV

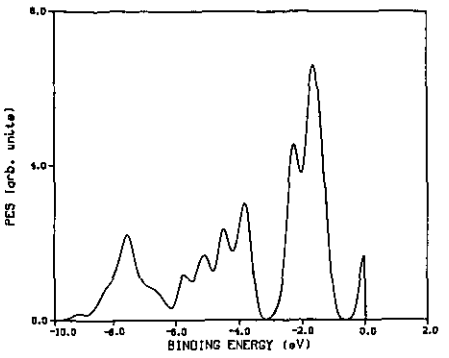

Figure 4. The spin- and angle-resolved PES corresponding to the $\overline{\Gamma}$ point in the surface Brillouin zone. Solid lines correspond to the majority-spin states and dashed lines the minority-spin states.

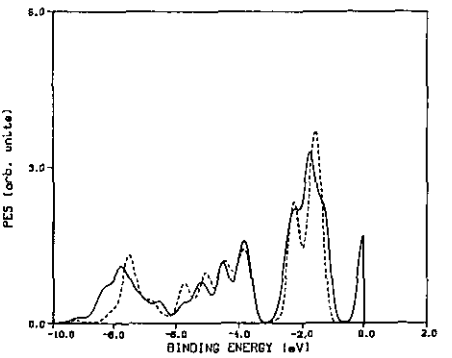

Figure 5. The spin- and angle-resolved PES corresponding to the $\overline{X}$ point in the surface Brillouin zone. Solid lines correspond to the majority-spin states and dashed lines the minority-spin states.

respectively. These two peaks have very weak spin polarizations and small exchange splittings. The satellite peak at around −8.0 eV has much higher intensity than the one in the $\overline{\Gamma}$ spectrum; it also has a large exchange splitting.

Table 6. The photoemission spectral weights projected onto the majority- and minority-spin states belonging to various irreducible representations. Both sets of the results calculated in the single-particle and many-body approach are listed.

	Single-particle PES weights		Many-body PES weights	
	Majority	Minority	Majority	Minority
$\overline{\Gamma}_1$	2.00	2.00	4.00	4.08
$\overline{\Gamma}_2$	4.00	4.00	2.04	2.04
$\overline{\Gamma}_3$, $\overline{\Gamma}_4$	4.00	4.00	4.05	4.05
$\overline{X}_1$	3.00	3.00	2.92	1.97
$\overline{X}_2$	2.00	2.00	3.07	1.98
$\overline{X}_3$, $\overline{X}_4$	4.00	4.00	3.92	3.88

As we have discussed above, many-body correlations can change the spectral weight distribution. It is interesting to have a more systematic study of the PES weight distribution. Shown in table 6 are the spin-resolved PES weights projected onto the states belonging to various irreducible representations, together with the one-particle results obtained from applying a Hubbard-model-like (mean-field) treatment to the interaction Hamiltonian, in which the single-particle energy levels are shifted by the exchange interaction into single-particle majority- and minority-spin levels. It can be clearly seen that many-body correlations yield pronounced redistribution of the spectral weights. Of particular interest is the increment in the *electronic* occupation at $\overline{X}_2$. This means that states that are nominally empty (or above the Fermi level) according to the single-particle calculations are actually occupied with appreciable probability by electrons.

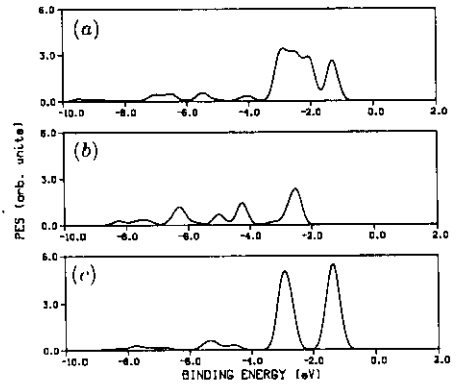

Figure 6. The angle-resolved PES projected onto states belonging to the $\overline{\Gamma}_1$ (*a*), $\overline{\Gamma}_2$ (*b*), and Γ_3, Γ_4 (*c*) representations.

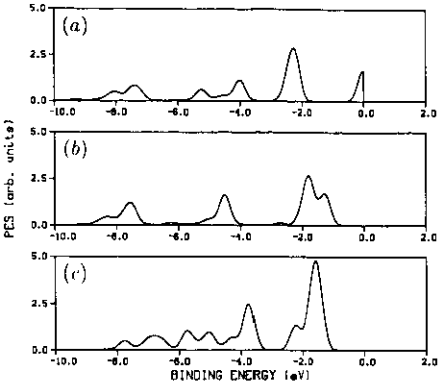

Figure 7. The angle-resolved PES projected onto states belonging to the $\overline{X}_1$ (*a*), $\overline{X}_2$ (*b*), and $\overline{X}_3$, $\overline{X}_4$ (*c*) representations.

To provide a better picture of the spectral weight redistribution, the energy resolved PES corresponding to the $\overline{\Gamma}$ and $\overline{X}$ point are presented in figures 6 and 7. These many-body results are *qualitatively* different from the single-particle ones (see tables 5 and 6) because in many-body systems configuration interactions mix all single-particle energy levels. A many-body theory is necessary to understand the photoemission spectrum and its implications on the many-body electronic structures of strongly correlated systems, such as the Ni(001) surface structure studied here.

6. Conclusions

The electronic structure of a strongly correlated transition-metal surface, a FCC Ni(001) surface, has been studied in an exactly soluble many-body periodic small-cluster approach. This approach incorporates both band-structure effects and many-body correlations on an equal footing. No perturbation theory was employed. The model is based on, but goes beyond, the local-density-approximation band-structure results. The anisotropic crystal-field and kinetic-energy effects at the surface have been taken into account. The solution provides accurate and detailed information about some important properties, particularly those induced by strong local many-body correlations.

The many-body electronic structure of the Ni(001) surface has been calculated. The exact finite-basis calculations provide the full description of both the eigenvalues and eigenstates for the ground state as well as all excited states (in the restricted finite-dimensional Hilbert space), allowing the determination of any desired (uniform and short-ranged) correlation functions. Energy-, spin-, and angle-resolved as well as integrated photoemission spectra have been obtained and compared with the bulk and thin-film results. Some unique features associated with the surface structure have been identified.

A surface-induced split-off peak with full spin polarization in majority-spin orientation has been observed at the Fermi level. It has the same origin as a similar peak found in the thin-film case [6]. However, the relative intensity of this peak and the overall distribution of the spectrum are quite different in the two cases due

to the modified single-particle electronic structure used in this work [21]. Detailed symmetry and energy level analysis shows that this peak comes completely from the contribution of the states of $\overline{X}_1$ symmetry. A qualitative deviation of the symmetry-projected spectral weight distribution from the single-particle results has been found. A satellite peak with overall spin polarization in majority-spin orientation and large exchange splitting has also been found at around 8.0 eV below the Fermi level. Surface-sensitive, angle- and spin-resolved photoemission experiments should be able to test our results.

The many-body electronic structure and photoemission spectrum reported in this contribution are quite interesting in its own right. Furthermore, these results may serve as a starting point for studies of more complex surface-related phenomena, e.g. surface adsorption and interface problems involving transition metals. The theory can be further improved by considering the many-body coupling between surface layers and the substrate. Work along these lines will be pursued in the near future.

Acknowledgments

This work was supported by Cray Research, Inc. and the University of Nevada, Las Vegas (UNLV). Computations were carried out on the Cray Y-MP at the National Supercomputing Center for Energy and the Environment (NSCEE) at UNLV. Technical assistance of the staff at NSCEE, particularly Sam West, is greatly appreciated.

References

[1] For a review, see, e.g.
Mathon J 1988 *Prog. Theor. Phys.* **51** 1
Jones R O and Gunnarsson O 1989 *Rev. Mod. Phys.* **61** 689
[2] Wang C S, Klein B N and Krakauer H 1985 *Phys. Rev. Lett.* **54** 1852
[3] Chen J, Singh D and Krakauer H 1988 *Phys. Rev.* B **38** 12 834
[4] Di Fabrizio E, Mazzona G, Petrillo C and Sacchetti F 1989 *Phys. Rev.* B **40** 9502
[5] See, for example
Norman M R 1990 *Phys. Rev. Lett.* **64** 1162, 2466; 1991 *Phys. Rev.* B **44** 1364
Anisimov V I, Zaanen J and Anderson O K 1991 *Phys. Rev.* B **44** 943 and references cited therein
[6] Chen Changfeng and Falicov L M 1989 *Phys. Rev.* B **40** 3560
[7] Chen Changfeng 1990 *Phys. Rev. Lett.* **64** 2176; 1991 *Phys. Rev.* B **43** 6347
[8] For a recent survey on this subject, see
Freericks J K and Falicov L M 1990 *Phys. Rev.* B **42** 4960
[9] Penn D 1979 *Phys. Rev. Lett.* **42** 921
Liebsch A 1979 *Phys. Rev. Lett.* **43** 1431
Davis L C and Feldkamp L A 1980 *Solid State Commun.* **34** 141
Kleinman L and Mednick K 1981 *Phys. Rev.* B **24** 6880
[10] Victora R H and Falicov L M 1985 *Phys. Rev. Lett.* **55** 1140
[11] Slater J C and Koster G F 1954 *Phys. Rev.* **94** 1498
Corrected and expanded to include f electrons by Sharma R R 1979 *Phys. Rev.* B **19** 2813
[12] Moruzzi V L, Janak J F and Williams A R 1978 *Calculated Electronic Properties of Metals* (New York: Pergamon)
[13] Dannan H, Heer R and Meyer A J P 1968 *J. Appl. Phys.* **39** 659
The measured Ni moment, $0.616\mu_B$, is believed to reflect a net spin imbalance of 0.56, with a g-factor of 2.2.
[14] Tinkham M 1964 *Group Theory and Quantum Mechanics* (New York: McGraw-Hill)

[15] A realistic surface U might become necessary for *very detailed* comparison with some experimentally observed features.

[16] A further improvement can be achieved by taking into account the distortion of charge distribution at (near) the surfaces.

[17] Bouckaert L P, Smoluchowsky R and Wigner E 1936 *Phys. Rev.* **50** 58

[18] Luehrmann A W 1968 *Adv. Phys.* **17** 1

[19] The split-off is caused by the fact that d orbitals, except the one with xy symmetry, experience the loss of neighbouring atoms and have a large downward energy shift.

[20] The MBDOS should not be confused with the usual single-particle DOS; here the eigenvalues are the energies of many-body states rather than single-particle excitation energies.

[21] From the bulk band structure for Ni, one also can predict a fully spin-polarized state in majority spin at X. The issue being addressed in this work is the modification caused by the presence of the surface and correlation effects.